Quantum measurements with superconducting circuits

Tanay Roy, A. M. Vadiraj, Madhavi Chand, A. Ranadive, Suman Kundu, Meghan P. Patankar and R. Vijay*

Quantum Measurement and Control Laboratory, Department of Condensed Matter Physics and Materials Science,
Tata Institute of Fundamental Research, Mumbai 400 005, India

We measure the state of a superconducting quantum bit (qubit) coupled to a microwave cavity by scattering a microwave signal from the cavity. The scattered signal is amplified using a low-noise Josephson parametric amplifier. We carried out measurements to infer the coherence properties of the qubit. In the strong measurement regime, we observe quantum jumps between the qubit states in real time, while we observe stochastic quantum trajectories in the weak measurement regime. The coherence times and measurement fidelity obtained are sufficient for implementing quantum error correction.

Keywords: Circuit QED, coherence properties, qubits, quantum measurement, superconducting circuits.

Introduction

THE past three decades have seen a tremendous rise in experiments probing the quantum nature of various atomic, photonic and solid-state systems. Though primarily driven by the promise of powerful quantum machines[1], these experiments are forcing us to revisit some of the very fundamental ideas and implications of quantum mechanics. The thought experiments put forth by the founding fathers of quantum physics have actually been implemented in the laboratory and have validated the often strange outcomes predicted earlier. A striking example is that of experiments probing single quantum degrees of freedom in contrast to earlier experiments which only looked at ensemble behaviour. Another example is the measurement process by which one obtains information about the state of the quantum system. The textbook picture is that of an instantaneous collapse of the wavefunction to an eigenstate of the observable. However, since any real experiment involving a quantum measurement takes a finite amount of time, the notion of weak measurements, where information about the quantum state is obtained slowly was introduced[2]. It is then natural to talk about the evolution of the quantum state during such a measurement. This problem is addressed in quantum optics using the notion of quantum trajectories[3,4] and has

been discussed more recently in the context of solid-state systems using the quantum Bayesian formalism[5]. In this picture, the quantum system undergoing measurement evolves slowly due to the back-action of the detector, until it ends up in one of the eigenstates of the measured observable. So it can be said that the collapse is gradual and the state evolution can be inferred from the detector output. It is now routinely possible to observe these effects in an experiment.

Superconducting circuits operating at millikelvin temperatures have emerged as a leading candidate for building quantum bits for a scalable architecture for quantum computing[6]. These circuits are fabricated using conventional nanolithographic techniques, and the control and measurement is implemented using microwave frequency signals. Over the last 15 years or so, tremendous progress has been made on various fronts, including coherence times, high-fidelity measurements and precise control. Apart from applications in quantum computing, superconducting circuits have been used in experiments in microwave quantum optics[7] with the ability to explore regimes not accessible in conventional quantum optics.

In this article, we will focus on quantum measurements implemented using superconducting circuits. In particular, we will focus on the circuit QED architecture[8,9], where a superconducting qubit is coupled to a microwave cavity to implement an ideal measurement Hamiltonian. This alows one to implement textbook quantum measurements relatively easily. Apart from the qubit and cavity, one also needs superconducting parametric amplifiers[10,11] in order to implement quantum measurements with high efficiency. The article is organized as follows. First, we will introduce the basics of superconducting qubits and the circuit QED architecture. We will go on to describe the quantum measurement process in the next section, with a particular focus on weak or partial measurements. Then, we will describe the experimental set-up and discuss some basic qubit measurements in the next section. Finally, we will conclude and discuss the challenges ahead.

Superconducting quantum circuits

Superconducting circuits consist of metallic films of a superconducting material like aluminium or niobium

patterned on a substrate. The patterns are designed to form different kinds of electrical circuit elements like inductors, capacitors, planar transmission lines and Josephson junctions. These components are combined to construct various types of resonators, which can be either linear or nonlinear. The nonlinearity is provided by a circuit element called the Josephson tunnel junction[12], which consists of two layers of a superconductor separated by a thin insulating layer. A supercurrent I can flow through such a junction, such that $I = I_0 \sin \delta$, while $V = \phi_0 \dot{\delta} / 2\pi$ is the voltage across the junction. Here, δ is the gauge-invariant phase difference across the junction and $\phi_0 = h/(2e)$ is the magnetic flux quantum. The Josephson junction can be thought of as a nonlinear inductor with an inductance $L_J(I) = L_{J0}(1 - I^2/I_0^2)^{-1/2}$, where $L_{J0} = L_J(0) = \phi_0/(2\pi I_0)$ is the linear part of the inductance. The Josephson junction is a remarkable device and is crucial for superconducting qubits as it is the only known device which can provide nonlinearity without dissipation at such low temperatures. The use of superconducting materials for these circuits ensures that all of these devices, when operated at dilution fridge temperatures (~10 mK), offer very low intrinsic dissipation even at microwave frequencies.

Various kinds of superconducting qubit designs exist[6], but the basic qubit can be thought of as a nonlinear quantum oscillator. This is true in particular for the so-called transmon qubit[13], which can be described as a weakly nonlinear oscillator. The design itself is quite simple and consists of a single Josepson junction shunted by a capacitor (C_J) as shown in Figure 1 a. The transition frequency between the ground and first excited states is approximately given by the linear resonant frequency $\omega_{01} \sim 1/(L_{J0}C_J)^{1/2}$, while the anharmonicity $\alpha = \omega_{01} - \omega_{12} \sim E_C$, where $E_C = e^2/(2C_J)$ is the charging energy[13]. The transition frequency can be made tunable by replacing the single junction with two junctions in a superconducing loop (Figure 2). Such a combination of junctions is called a superconducting quantum interference device (SQUID) and implements a tunable inductance which can be varied with the help of an external magnetic flux. Though the
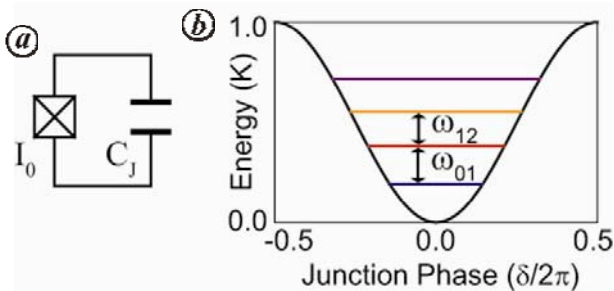
transmon has several low-lying energy levels (Figure 1 b), the anharmonicity $\alpha \sim 250$ MHz is sufficient to use it as a qubit by selectively addressing the ω_{01} transition using appropriately shaped microwave frequency pulses. Other kinds of qubits are constructed by choosing different combinations of the three basic circuit elements, i.e. inductor, capacitor and the Josephson junction[6], and provide different types of quantum-level structures. The transmon qubit is currently the most popular qubit providing reproducible performance, good coherence times and insensitivity to charge noise, and is extensively used for quantum information processing applications[14,15].

Circuit QED (cQED)[8] is the circuit implementation of the cavity QED architecture[16]. In cavity QED, a single atom interacts coherently with the electromagnetic field inside a Fabry–Perot cavity, whereas in cQED a superconducting qubit interacts coherently with an on-chip superconducting resonator[9] or a waveguide cavity[17]. Figure 2 shows the basic cQED set-up. This interaction is described by the Jaynes–Cummings Hamiltonian

$$H = \frac{\hbar\omega_{01}}{2}\sigma_z + \hbar\omega_c\left(a^\dagger a + \frac{1}{2}\right) + \hbar g(a\sigma^+ + a^\dagger\sigma_-), \qquad (1)$$

where the first term represents the qubit as a pseudo-spin (Pauli spin operator), the second term represents the electromagnetic cavity and the third term is the interaction between the qubit and the electromagnetic field in the rotating wave approximation. Here ω_{01} is the transition frequency between the qubit levels, ω_c is the cavity mode frequency, g is the coupling strength between the qubit and cavity mode and $\sigma_\pm = (\sigma_x \pm i\sigma_y)/2$ are the qubit raising and lowering operators. For measurement, the qubit frequency is far detuned from the cavity frequency and in this dispersive regime ($\Delta = \omega_{01} - \omega_c \gg g$), the Hamiltonian reduces to

$$H = \frac{\hbar\omega_{01}}{2}\sigma_z + \hbar(\omega_c + \chi\sigma_z)\left(a^\dagger a + \frac{1}{2}\right), \qquad (2)$$

where χ is called the dispersive shift. Since the cavity resonant frequency depends on the qubit state, a quantum

Figure 1. a, Circuit diagram of a transmon qubit. It consists of a Josephson junction shunted by a capacitor. b, First four energy levels of a transmon qubit. Since the potential is anharmonic, the energy levels are unequally spaced enabling one to isolate the bottom two levels to form a quantum bit (qubit).
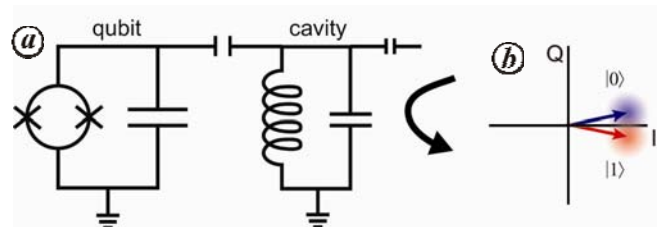
Figure 2. a, Circuit QED set-up consisting of a transmon qubit dispersively coupled to a single mode of an electromagnetic. The cavity resonance is shifted by a change in the qubit state. b, Consequently, a microwave signal probing the cavity acquires a qubit state-dependent phase shift, shown as two phasors in the I–Q plane.

state measurement can be implemented by probing the cavity with a microwave signal close to cavity resonant frequency. The scattered microwave signal acquires a qubit state-dependent phase shift which can be measured using a homodyne set-up. In addition to providing a mechanism for measurement, the cavity also protects the qubit by decoupling it from the environment. Since the qubit is coupled to the environment via the cavity, the cavity acts like a filter and helps in enhancing the lifetime of the qubit[18].

Quantum measurements

We now discuss the measurement process in a little more detail. We start by considering the measurement Hamiltonian in eq. (2). The first thing to notice is that the qubit–cavity coupling term $(\propto \sigma_z a^\dagger a)$ commutes with the bare qubit evolution Hamiltonian $(\propto \sigma_z)$. This implies that the eigenstates of the measurement operator are also the eigenstates of the qubit. Such measurements are called quantum non-demolition measurements and the qubit ends up in the eigenstate corresponding to the eigenvalue obtained in the measurement. The interaction term results in the entanglement between the qubit and the coherent state in the energized cavity. The measurement apparatus actually detects the coherent state (often called the pointer) which leaks out of the cavity. If the two are perfectly entangled, the detection of the coherent state in one of the two possible phases will project the qubit into the corresponding eigenstate. Such a situation corresponds to the strong or projective measurement in quantum mechanics. This requires that the coherent states corresponding to the two qubit states are perfectly resolved, which in practice means that we need to resolve the phase shift of the scattered microwave signal in a given measurement time.

There are four quantities which determine whether the phase shifts corresponding to the ground and excited states can be resolved. The first is the magnitude of the phase shift ($\Delta\phi$) which is set by the dispersive shift χ and the linewidth κ of the cavity. These quantities are fixed by design and cannot typically be varied in a given experiment. The second quantity is the magnitude of the microwave signal used to probe the cavity, since it is easier to resolve the phase shift of a larger signal. A related quantity is the noise in the phase measurement which could be due to the measurement set-up, but more fundamentally due to the quantum uncertainty in resolving the phase of the coherent state. Finally, there is the measurement or integration time, since a longer integration time, (averaging) will lead to better phase resolution. In practice, such measurements will yield a distribution of values for the phase which can be represented as two Gaussians centred at phase ϕ_{m0} and ϕ_{m1} corresponding to the ground and excited states of the qubit respectively. If

the two distributions have little or no overlap as shown in Figure 3 a, the measurement will be called a strong or projective measurement. In each measurement, we can determine which distribution the measured value of phase came from with no ambiguity. Hence, we can assign the value 0 or 1 to the measurement result corresponding to the qubit state $|0\rangle$ or $|1\rangle$.

Let us now consider what would happen if the distributions looked like those shown in Figure 3 b. This can be achieved experimentally by either reducing the magnitude of the microwave signal or by reducing the integration time. In a single measurement of this type, we can no longer assign the measured phase to one of the two histograms. Such measurements are called weak or partial measurements[2,3], since the measurement is not complete. This also implies that the qubit is not projected to one of its eigenstates in such partial measurements. Another point to note is that increasing the time of integration can take you from overlapping distributions (Figure 3 b) to well-resolved distributions (Figure 3 a), i.e. from weak to strong measurements. This means that a sequence of weak measurements can be equal to a strong measurement and both types of measurement are just two regimes of the same process.

Since the partial measurement does not give a binary result, but instead gives a range of random measurement outcomes, can we still say something about the qubit state after such a measurement? The answer is yes and we use the Bayesian formalism[19] to describe the procedure. We start by considering an example where we know the initial wavefunction $|\psi\rangle = \alpha|0\rangle + \beta|1\rangle$ describing the qubit state, such that $|\alpha|^2 + |\beta|^2 = 1$. We now perform a weak measurement which yields a value ϕ_m. The qubit state ($|\psi'\rangle = \alpha'|0\rangle + \beta'|1\rangle$), after the weak measurement is given
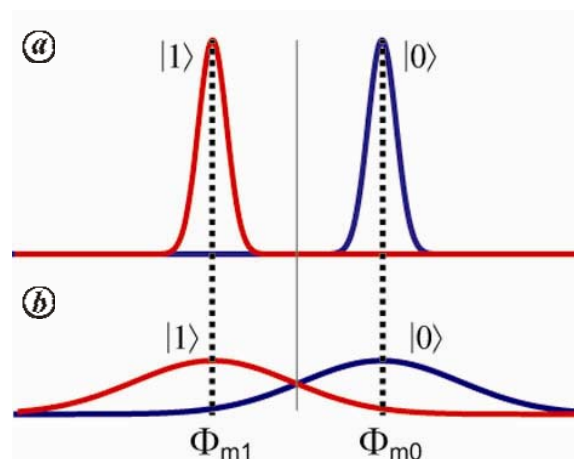

Figure 3. Histograms representing the distribution of phase values (ϕ_m) when a measurement is made in the cQED architecture. The two distributions correspond to the qubit prepared in the ground (centred at ϕ_{m0}) and excited states (centred at ϕ_{m1}) respectively. **a**, Strong measurement where the two histograms are well separated. **b**, Partial or weak measurement with overlapping distributions.

by the following formula which resembles the Bayes theorem for probabilities

$$P(0 \mid \phi_m) = \frac{P(0)P(\phi_m \mid 0)}{P(\phi_m)}, \qquad (3)$$

where $P(0|\phi_m) = |\alpha'|^2$ is the conditional probability that the qubit is in state 0 after a weak measurement yields the result ϕ_m, $P(0) = |\alpha|^2$ and $P(1) = |\beta|^2$ are the initial qubit state probabilities, while $P(\phi_m|0)$ and $P(\phi_m|1)$ are the measurement distributions as shown in Figure 3 b. $P(\phi_m) = P(0)P(\phi_m|0) + P(1)P(\phi_m|1)$ is the probability of getting the weak measurement result ϕ_m. The coefficient $|\beta'|^2$ is determined by normalization, while the relative phase between α' and β' is the same as for α and β, since the measurement reveals no information about the relative phase[19]. In this description we have implicity assumed that the state remains pure after weak measurement, but that is true only if the quantum efficiency of the measurement is unity[20,21]. This is equivalent to saying that the width of the measurement histogram (Figure 3 b) is set by quantum uncertainty and not due to technical noise in the measurement set-up. In superconducting architecture, this is achieved using phase-sensitive Josephson parametric amplifiers (JPA)[11] which can provide near noiseless amplification of a single quadrature of a microwave signal[22,23], allowing one to get close to unit quantum efficiency. When that is achieved, and if the initial state is pure, the qubit state remains pure throughout the measurement process, i.e. the wavefunction can be tracked from its initial state to its final state during the process of measurement. Note that the result of a weak measurement is random and hence the qubit state evolution is stochastic under a sequence of weak measurements[21,24]. This formula is still applicable when the initial state of the qubit can only be represented by a density matrix. The conditional probability $P(0|\phi_m)$ now relates to the diagonal elements of the density matrix[21]. If ρ and ρ' represent the density matrix of the qubit before and after a weak measurement, they are related by,

$$\rho'_{11} = \frac{\rho_{11}P(\phi_m \mid 1)}{P(\phi_m)}, \quad \rho'_{00} = \frac{\rho_{00}P(\phi_m \mid 0)}{P(\phi_m)}, \qquad (4)$$

$$\rho'_{01} = \rho_{01}\frac{\sqrt{\rho'_{11}\rho'_{00}}}{\sqrt{\rho_{11}\rho_{00}}}. \qquad (5)$$

Experimental set-up and measurements

We now describe the experimental set-up and discuss some basic qubit characterization measurements. The devices are made using standard e-beam lithography on high-resistivity silicon or sapphire substrates. Thin films

of aluminium (~30–100 nm) are deposited using an e-beam evaporator at a pressure of about 10^{-7} mBar. For circuits containing Josephson junctions, double-angle evaporation utilizing a Dolan bridge technique is used to get two overlapping aluminium films. Oxygen is introduced into the evaporator chamber before the second evaporation to oxidize the surface of the aluminium film which forms a thin tunnel barrier.

Figure 4 shows a detailed schematic of the measurement set-up. In our experiments, the transmon qubit is placed inside a copper waveguide cavity implementing the 3D transmon architecture[17]. These are then anchored to the base plate of a cryofree dilution refrigerator. Heavily attenuated and filtered coaxial lines bring microwave signals from room-temperature apparatus to excite the qubit and cavity. The output of the cavity goes through a low-pass filter, an isolator and a directional coupler, where it is combined with a strong microwave tone used for energizing the JPA. The combined signal is sent to the JPA, which amplifies the chosen quadrature of the measurement signal[23]. The amplifed signal reflects off the JPA and via the circulator goes to the output line, where it is further amplified (~80 dB) before it reaches the homodyne set-up at room temperature. The homodyne set-up consists of a microwave generator which creates the measurement signal that is split into two parts. One part goes to the cavity, while the other drives the LO (local oscillator) port of a mixer. The amplified signal from the cavity is sent to the radio frequency (RF) port of the mixer which multiplies the LO and RF signals and outputs the in-phase (I) and quadrature-phase (Q) components of the measurement signal. Both signals (I, Q) are then digitized and processed on a computer to extract the amplitude and phase of the measurement signal. A second generator is used to create the microwave signals at the qubit transition frequency ω_{01} and is combined with the measurement signal before it goes to the qubit–cavity system. The continuous microwave signals from the generators are modulated with the help of mixers and arbitrary waveform generators to create appropriate pulses for qubit manipulation and measurement.

We now describe some basic qubit characterization experiments[25,26]. The first experiment typically used to characterize a qubit is to drive it resonantly at its transition frequency ω_{01} and observe coherent Rabi oscillations between the two states. When driven on resonance, the qubit state evolves in a sinusoidal manner and oscillates between the ground and excited states at a rate that is proportional to the drive amplitude. The Rabi oscillation experiment proceeds by sending a variable width microwave pulse at ω_{01} followed by projective measurement. This is repeated several thousand times to create an ensemble average as shown in Figure 5, where the coherent oscillations are clearly visible. The y-axis here is a voltage proportional to the phase shift in the measurement signal between the ground and excited states of the qubit
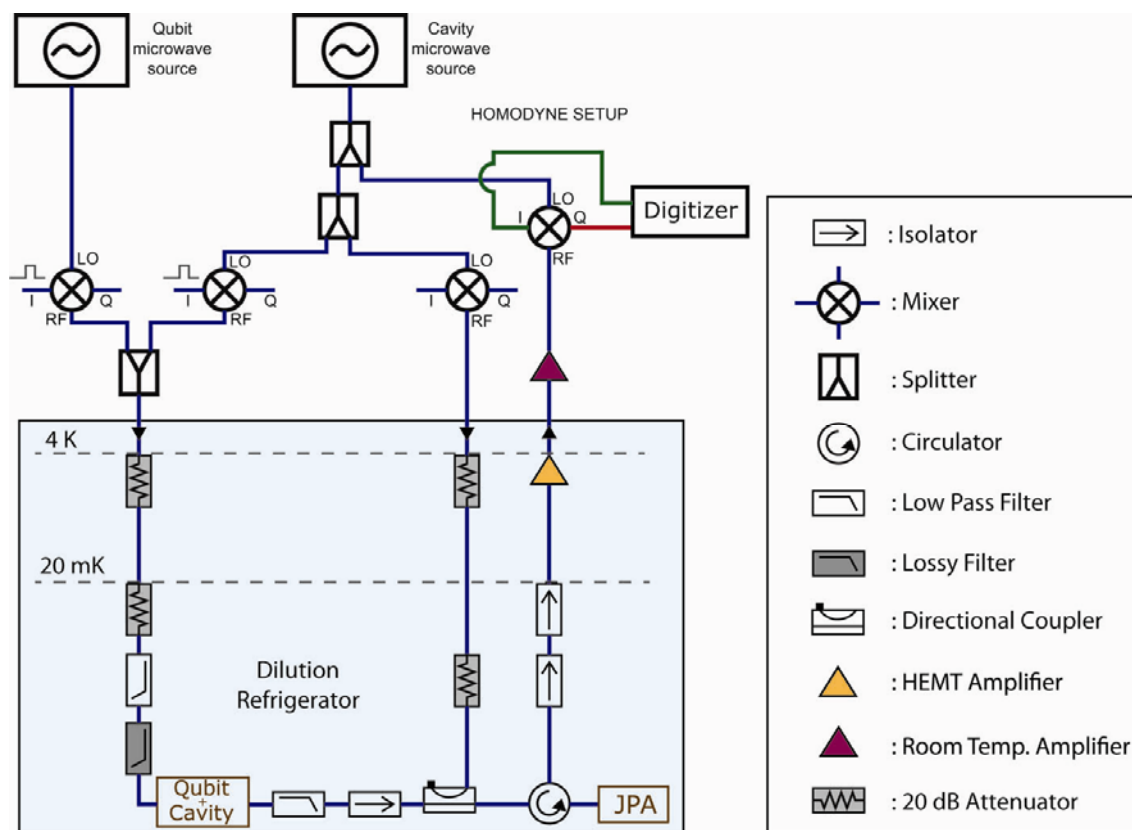
Figure 4. A detailed schematic of the measurement set-up showing both the room temperature signal generation and detection setup (top) and the cryogenic set-up (bottom). The qubit and cavity are anchored to the base temperature plate (20 mK) of the dilution refrigerator.
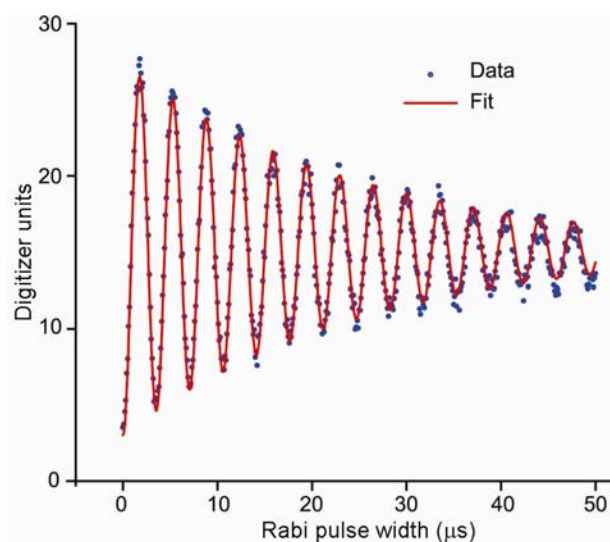

Figure 5. Coherent oscillations in the qubit state population as a function of pulse width of the resonant microwave drive. The Rabi oscillation amplitude shows an exponential decay with a decay constant $T_R = 25$ μs.

and is represented in digitizer units. The oscillations decay with a characteristic time constant $T_R = 25$ μs. The decay is due to a combination of qubit relaxation and

other noise at the Rabi frequency[26]. The main purpose of this experiment is to calibrate the pulse required to put the qubit in the excited state (π pulse) or a 50–50 superposition state ($\pi/2$ pulse).

With a calibrated π pulse, we can now measure the relaxation time of the qubit from its excited state. This experiment proceeds by preparing the qubit in its excited state and then waiting some time before making a measurement. By repeating this experiment several thousand times for different delays between the π pulse and the measurement pulse, we obtain an ensemble averaged curve as shown in Figure 6. We can observe an exponential decay with a decay constant given by $T_1 = 20$ μs, which is the excited state lifetime.

Another important timescale is associated with the dephasing process, which scrambles the relative phase of a superposition state due to noise that affects the qubit transition frequency ω_{01}. This timescale is probed with the Ramsey oscillation experiment which proceeds as follows. We first send a $\pi/2$ pulse to prepare a 50–50 superposition state, but the pulse is created at a slightly detuned frequency $\omega_{01} - \Omega$. As described above, this pulse is also calibrated using the Rabi oscillation experiment, but with a detuned drive. A second $\pi/2$ pulse is then sent to the qubit after a variable time delay $\Delta\tau$ and immediately

followed by a measurement pulse. Since the microwave pulse is detuned from resonance, the relative phase of the superposition evolves at the detuning frequency Ω in a frame rotating at ω_{01}. The time delay $\Delta\tau$ determines how the state would transform due to the second $\pi/2$ pulse. The ensemble averaged result of such an experiment is shown in Figure 7. We observe a sinusoidal oscillation at frequency Ω with an amplitude decay constant $T_2 = 30$ µs. The oscillations decay due to a combination of qubit relaxation and low frequency noise in ω_{01}. In the absence of any noise in ω_{01}, $T_2 = 2T_1$. In general,

$1/T_2 = 1/(2T_1) + 1/T_\varphi$, where T_φ is called the dephasing time[26] and is associated with the decay due to noise in ω_{01} only. For this experiment, $T_\varphi = 120$ µs. These experiments characterize the coherence properties of superconducting qubits and the numbers obtained are typical for a transmon-type qubit in a 3D waveguide cavity[17].

The measurements discussed so far were ensemble averaged measurements which were used to characterize the coherence properties of qubits. The signal-to-noise ratio in typical cQED set-ups which do not use a parametric amplifier is not sufficient to reveal adequate information
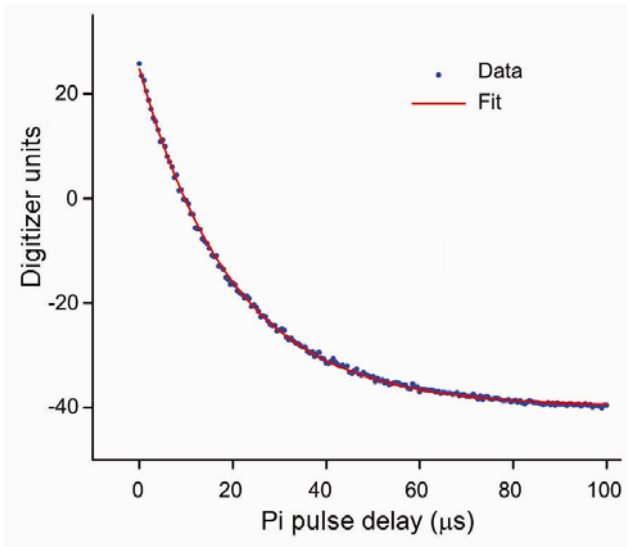

Figure 6. The exponential decay of the excited state population as a function of the delay time between the π pulse and measurement. The decay constant $T_1 = 20$ µs.
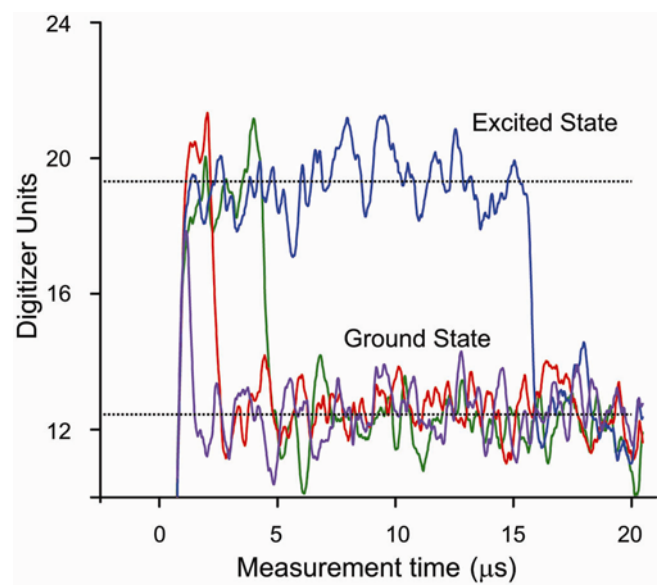

Figure 8. Four individual single-shot measurement traces taken with the qubit prepared in the excited state. Stochastic quantum jumps due to spontaneous relaxation are clearly visible.
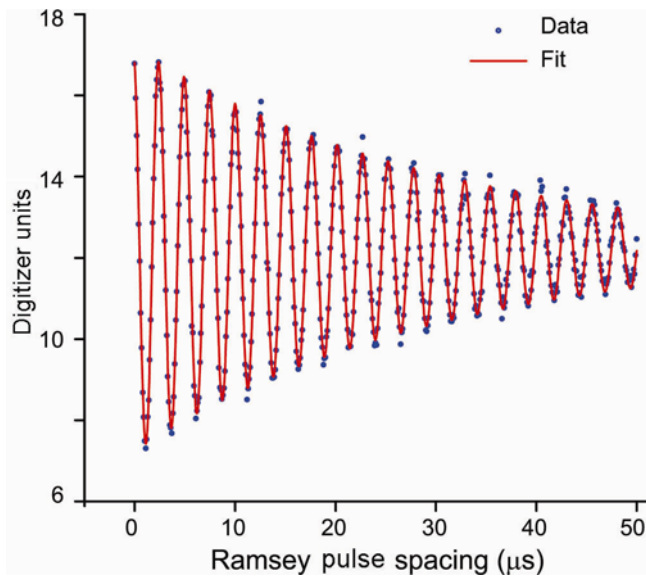

Figure 7. Ramsey oscillations in the qubit state population as a function of the pulse spacing between two detuned $\pi/2$ pulses. The Ramsey oscillation amplitude shows an exponential decay with a decay constant $T_2 = 30$ µs.
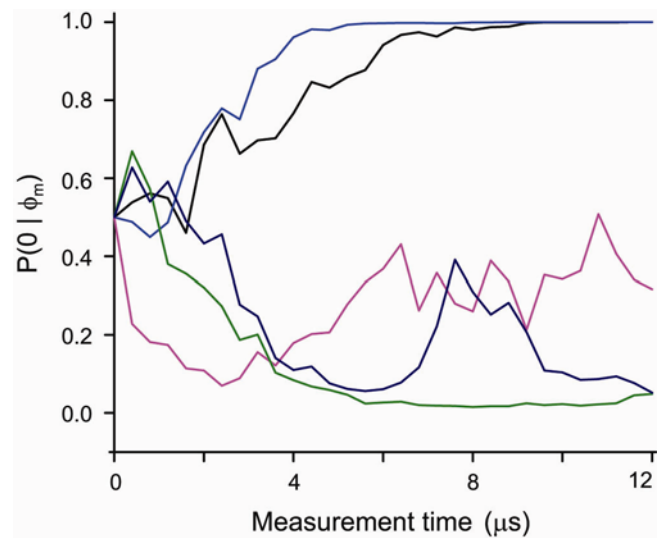

Figure 9. Five individual quantum trajectories of a qubit prepared in a 50–50 superposition state. The stochastic nature of evolution of qubit from its initial superposition state to its final eigenstate under weak measurement is clearly visible.

in a single measurement. The high-gain (20 dB) and near-quantum limited noise of JPAs[10,11] is crucial for single-shot measurements. Figure 8 shows four measurement traces taken with the qubit prepared in the excited state. The dashed lines indicate the mean level corresponding to the ground and excited states. We note that the two levels can be resolved in a very short period of time, indicating very high signal-to-noise ratio. Further, we observe the real-time relaxation of the qubit from its excited state to its ground state, the so-called quantum jumps[22]. The different traces show the jumps at different times, since relaxation is a stochastic process. The mean time of the jump will however be related to the relaxation time T_1 (ref. 22). The magnitude of the microwave signal used to probe the cavity was chosen to be sufficiently high so that the two states could be resolved in a short period of time, i.e. the strong measurement regime. We next look at the case where we turn down the measurement strength so that the projection time is longer. First we obtain histograms for qubit states 0 and 1 (as in Figure 3 b) corresponding to a specific measurement strength and integration time. Next we prepare the qubit in a known initial state and record the output signal while applying a long measurement tone of the same strength. We then analysed the output signal in this weak measurement regime using eq. (3) by breaking down the entire measurement signal into smaller time bins. Each time bin corresponds to one weak measurement and we update the quantum state after each step. The resulting quantum trajectories[21] are shown in Figure 9 for five separate iterations, in each of which the qubit was initially prepared in a 50–50 superposition state. Note the stochastic evolution of the qubit state and its progression towards its eigenstates. Since the initial qubit state was a 50–50 superposition, the final qubit state after a sufficiently long time was also distributed equally.

Conclusion

We have characterized the coherence properties of a transmon qubit coupled to a copper waveguide cavity. We obtained a relaxation time $T_1 = 20$ μs and a dephasing time $T_\varphi = 120$ μs. Further, we used JPAs to implement single-shot measurement of the qubit state and observed quantum jumps. By turning down the microwave power used to probe the cavity, we explored the weak measurement regime and observed the stochastic evolution of the quantum state. These initial measurements are essential steps for progressing towards the realization of a practical quantum processor. A crucial goal for the near term is the implementation of quantum error correction[27]. Even though the coherence times of superconducting qubits have improved by nearly five orders of magnitude[6] in the last 15 years, one needs the ability to preserve an arbitrary quantum state for indefinite lengths of time. The idea behind quantum error correction[27] is to distribute the quantum information amongst multiple entangled physical qubits to implement a single perfect logical qubit. This is possible because one can use a special type of measurement (syndrome) to detect errors on individual physical qubits without revealing information about the encoded quantum state. Once detected, the errors can be corrected, thus restoring the system to its original state. A basic requirement is to have qubits with small enough error rates and the coherence times in superconducting qubits have just about reached that threshold. Several proof of principle experiments have already been implemented[14,15,28–30], but a full demonstration of quantum error correction still remains a challenge. A massive effort is underway to reach this important milestone towards building a quantum processor.

1. Nielsen, M. and Chuang, I., *Quantum Computation and Quantum Information*, Cambridge University Press, 2000.
2. Braginsky, V. B. and Khalili, F. Ya., Quantum nondemolition measurements: the route from toys to tools. *Rev. Mod. Phys.*, 1996, **68**(1), 1–11.
3. Gardiner, C. and Zoller, P., *Quantum Noise*, Springer, 2004.
4. Goan, H.-S., Milburn, G. J., Wiseman, H. M. and Sun, H. B., Continuous quantum measurement of two coupled quantum dots using a point contact: a quantum trajectory approach. *Phys. Rev. B*, 2001, **63**(12), 125326-1 to 12.
5. Korotkov, A. N., Continuous quantum measurement of a double dot. *Phys. Rev. B*, 1999, **60**(8) 5737–5742.
6. Devoret, M. H. and Schoelkopf, R. J., Superconducting circuits for quantum information: an outlook. *Science*, 2013, **339**(6124), 1169–1174.
7. You, J. Q. and Nori, F., Atomic physics and quantum optics using superconducting circuits. *Nature*, 2011, **474**(7353), 589–597.
8. Blais, A., Huang, R.-S., Wallraff, A., Girvin, S. M. and Schoelkopf, R. J., Cavity quantum electrodynamics for superconducting electrical circuits: an architecture for quantum computation. *Phys. Rev. A*, 2004, **69**(6), 062320-1 to 14.
9. Wallraff, A. *et al.*, Strong coupling of a single photon to a superconducting qubit using circuit quantum electrodynamics. *Nature*, 2004, **431**(7005), 162–167.
10. Castellanos-Beltran, M. A., Irwin, K. D., Hilton, G. C., Vale, L. R. and Lehnert., K. W., Amplification and squeezing of quantum noise with a tunable Josephson metamaterial. *Nature Phys.*, 2008, **4**(12), 929–931.
11. Hatridge, M., Vijay, R., Slichter, D. H., Clarke, J. and Siddiqi, I., Dispersive magnetometry with a quantum limited SQUID parametric amplifier. *Phys. Rev. B*, 2011, **83**(13), 134501-1 to 8.
12. Josephson, B. D., Coupled superconductors. *Rev. Mod. Phys.*, 1964, **36**(1), 216–220.
13. Koch, J. *et al.*, Charge-insensitive qubit design derived from the Cooper pair box. *Phys. Rev. A*, 2007, **76**(4), 042319-1 to 19.
14. Kelly, J. *et al.*, State preservation by repetitive error detection in a superconducting quantum circuit. *Nature*, 2015, **519**(7541), 66–69.
15. Córcoles, A. D., Magesan, E., Srinivasan, S. J., Cross, A. W., Steffen, M., Gambetta, J. M. and Chow, J. M., Demonstration of a quantum error detection code using a square lattice of four superconducting qubits. *Nature Commun.*, 2015, **6**, 6979-1 to 10.
16. Berman, P. (ed.), *Cavity Quantum Electrodynamics*, Academic Press, 1994.
17. Paik, H. *et al.*, Observation of high coherence in Josephson junction qubits measured in a three-dimensional circuit QED architecture. *Phys. Rev. Lett.*, 2011, **107**(24), 240501-1 to 5.

18. Houck, A. A. *et al.*, Controlling the spontaneous emission of a superconducting transmon qubit. *Phys. Rev. Lett.*, 2008, **101**(8), 080502-1 to 4.

19. Korotkov, A. N., Quantum Bayesian approach to circuit QED measurement. arXiv:1111.4016[quant-ph].

20. Hatridge, M. *et al.*, Quantum back-action of an individual variable-strength measurement. *Science*, 2013, **339**(6116), 178-181.

21. Murch, K. W., Weber, S. J., Macklin, C. and Siddiqi, I., Observing single quantum trajectories of a superconducting qubit. *Nature*, 2013, **502**(7470), 211–214.

22. Vijay, R., Slichter, D. H. and Siddiqi, I., Observation of quantum jumps in a superconducting artificial atom. *Phys. Rev. Lett.*, 2011, **106**(11), 110502-1 to 4.

23. Vijay, R. *et al.*, Stabilizing Rabi oscillations in a superconducting qubit using quantum feedback. *Nature*, 2012, **490**(7418), 77–80.

24. Weber, S. J., Chantasri, A., Dressel, J., Jordan, A. N., Murch, K. W. and Siddiqi, I., Mapping the optimal route between two quantum states. *Nature*, 2014, **511**(7511), 570–573.

25. Collin, E., Ithier, G., Aassime, A., Joyez, P., Vion, D. and Esteve, D., NMR-like control of a quantum bit superconducting circuit. *Phys. Rev. Lett.*, 2004, **93**(15), 157005-1 to 4.

26. Ithier, G. *et al.*, Decoherence in a superconducting quantum bit circuit. *Phys. Rev. B*, 2005, **72**(13), 134519-1 to 22.

27. Terhal, B. M., Quantum error correction for quantum memories. *Rev. Mod. Phys.*, 2015, **87**(2), 307–346.

28. Fedorov, A., Steffen, L., Baur, M., Da Silva, M. P. and Wallraff, A., Implementation of a Toffoli gate with superconducting circuits. *Nature*, 2011, **481**(7380), 170-172.

29. Reed, M. D., DiCarlo, L., Nigg, S. E., Sun, L., Frunzio, L., Girvin, S. M. and Schoelkopf, R. J., Realization of three-qubit quantum error correction with superconducting circuits. *Nature*, 2012, **482**(7385), 382–385.

30. Ristè, D., Poletto, S., Huang, M.-Z., Bruno, A., Vesterinen, V., Saira, O.-P. and DiCarlo, L., Detecting bit-flip errors in a logical qubit using stabilizer measurements. *Nature Commun.*, 2015, **6**, 6983-1 to 6.